Intense-field molecular spectroscopy: Vibrational and rotational effects in harmonic generation by H_2^+

E. E. Aubanel, T. Zuo, and A. D. Bandrauk
Laboratoire de Chimie Théorique, Faculté des Sciences, Université de Sherbrooke, Sherbrooke, Québec, Canada J1K 2R1
(Received 16 December 1993)

We present results of a complete treatment of electronic, vibrational, and rotational motion in numerical calculation of harmonic generation (HG) of 1064-nm laser radiation by the H_2^+ molecular ion for intensities $10^{13} \leq I \leq 10^{14}$ W/cm^2. We show that efficient HG can be enhanced by suppression of photodissociation, a phenomenon which results from vibrational trapping in laser-field-induced potential wells. The HG spectra exhibit peaks clustered around even and odd harmonic orders. All peaks can be assigned to Raman-like transitions between dressed eigenstates of the field-molecule system. Rotational excitation is shown to compete with HG. Thus harmonic generation and photon scattering in molecules holds the promise of a potential diagnostic for molecular stabilization by intense laser fields.

PACS number(s): 33.80.Gj, 33.10.−n, 33.90.+h, 42.50.Hz

I. INTRODUCTION

Recent theoretical work has shown that two-level systems can generate high harmonics of the fundamental laser frequency [1–4]. Odd-charged homonuclear diatomic ions have charge-resonance states [5] (e.g., the $1s\sigma_g$ and $2p\sigma_u$ states of H_2^+), which are strongly coupled by the field due to asymptotically diverging transition moments [$\mu(R) = eR/2$]. If these states are isolated, and if the laser frequency is comparable to the separation of the charge resonance states, then a low energy plateau (up to $\sim$ 10th order in 1064-nm radiation at 10^{13} W/cm^2 by H_2^+) of the harmonic generation (HG) spectrum appears which can be reproduced well by a two-level model [1].

Previous work has only dealt with the electronic motion, i.e., the nuclei were held fixed in exact numerical solution of the electronic motion [1], or a two-level analytic model was employed [1–4]. This should be a good approximation in the case of ions of heavy diatomic molecules such as I_2 exposed to short pulses [2,3]. However, for longer pulses or lighter ions, vibrational and rotational motion must be taken into account, and as we will show, contribute to the structure of the HG spectrum. In particular, *laser-induced avoided crossings* considerably modify the electronic potentials and as a consequence also the nuclear motion. Thus new nuclear bound states can be created by vibrational trapping in new laser-induced adiabatic wells [6–10]. The stability of such laser-induced nuclear states has been described earlier by Bandrauk and co-workers, based on the analogy to molecular predissociation [7–9]. The same group had also earlier proposed the detection of such laser-induced states in resonance Raman scattering spectra [10]. In the present work we compare results of a purely electronic treatment (i.e., static nuclei) with a two-electronic-state treatment including vibrational and rotational degrees of freedom, in calculation of the harmonic generation of 1064-nm laser radiation by H_2^+. We show that harmonic generation can serve as a measure of the structure of laser-induced nuclear states propagating on field-modified electronic surfaces.

The outline of the paper is as follows: in Sec. II we present a theoretical treatment of harmonic generation in H_2^+, showing that it results from transitions between Floquet states. In Sec. III we present results of calculations of harmonic generation by nonrotating H_2^+, and show that efficient HG is linked to supression of photodissociation or equivalently, stabilization of the molecular ion. In Sec. IV we present results of HG by H_2^+ which include rotation. A concluding discussion then follows in Sec. V.

II. THEORY

We will consider a two-electronic-state rotationless model of a homonuclear diatomic ion, such as the $^2\Sigma_g^+$ and $^2\Sigma_u^+$ states of H_2^+. One must solve the two coupled time-dependent Schrödinger equations for the nuclear states $\chi(R,t) = (\chi_1(R,t), \chi_2(R,t))$ (corresponding to electronic states $^2\Sigma_g^+$ and $^2\Sigma_u^+$, respectively):

$$\left[i\hbar \frac{\partial}{\partial t} + \frac{\hbar^2 \nabla^2}{2m} \right] \chi(R,t) = \begin{bmatrix} V_g(R) & V_{gu}(R,t) \\ V_{gu}(R,t) & V_u(R) \end{bmatrix} \chi(R,t), \tag{1}$$

where $V_{gu}(R,t) = \hbar\Omega_R(R) f(t) \cos(\omega t)$, $f(t)$ is the laser pulse shape, and Ω_R the Rabi frequency

$$\hbar\Omega_R(\text{eV}) = 1.45 \times 10^{-7} [I \text{ (W/cm}^2)][d \text{ (a.u.)}], \tag{2}$$

where I is the laser intensity and $[d \text{ (a.u.)}] = R/2$ is the $1\sigma_g \rightarrow 1\sigma_u$ transition moment in atomic units, which diverges with increasing internuclear distance [5]. Bandrauk and co-workers first pointed out the importance of

such large transition moments in creating nonlinear nonperturbative effects such as laser-induced avoided crossings [7–9]. For a periodic field, i.e., $f(t) = \text{const}$, the solutions of Eq. (1) are given by Floquet states:

$$|\psi_k(r,R,t)\rangle = e^{-i\epsilon_k t/\hbar}\sum_{n=-\infty}^{\infty} e^{in\omega t}\sum_{\alpha=1}^{N_\alpha} \times[d_{1,n}^{\alpha}(\epsilon_k)|\phi_g(r,R)\rangle|\chi_1^{\alpha}(R)\rangle + d_{2,n}^{\alpha}(\epsilon_k)|\phi_u(r,R)\rangle|\chi_2^{\alpha}(R)\rangle], \tag{3}$$

where for simplicity we have expanded the ground and excited nuclear wave functions into an equal number N_α of basis states, ϵ_k is the kth eigenvalue ($k = 0, \pm 1, \ldots, \pm\infty$), or *quasienergy*, of the time-independent Floquet Hamiltonian H_F, which has diagonal elements $E_1^{\alpha} + n\hbar\omega, E_2^{\alpha} + n\hbar\omega$ ($E_1^{\alpha}, E_2^{\alpha}$ are energies of zero-field nuclear eigenstates $|\chi_1^{\alpha}\rangle$, $|\chi_2^{\alpha}\rangle$ corresponding to electronic states $\phi_g(r,R)$ ($^2\Sigma_g^+$) and $\phi_u(r,R)$ ($^2\Sigma_u^+$), respectively) and off-diagonal elements

$$\begin{aligned} V_{1,n\pm1,2,n}^{\beta,\alpha} &= \langle\phi_g(r,R)|\langle\chi_1^{\beta}(R)|z|\chi_2^{\alpha}(R)\rangle|\phi_u(r,R)\rangle_{r,R}\mathcal{E}_0 \\ &= \langle\chi_1^{\beta}(R)|(R/2)|\chi_2^{\alpha}(R)\rangle\mathcal{E}_0 \\ &= \mu_{1,\beta,2,\alpha}\mathcal{E}_0, \end{aligned} \tag{4}$$

where R is the internuclear distance, r is the electronic coordinate, z is the projection of r on the internuclear axis, and $\mathcal{E}_0$ is the field strength. In Eq. (3), $d_{1,n}^{\alpha}(\epsilon_k)$ is the $d_{1,n}^{\alpha}$ (basis element of H_F) component of the eigenvector of H_F corresponding to eigenvalue ϵ_k. Note that since basis elements $d_{1,n}^{\alpha}$ are coupled only to functions $d_{2,n\pm1}^{\beta}$ by the Floquet matrix H_F, one can separate two noninteracting parts of Eq. (3):

$$|\psi_{2k+1}^{-}(r,R,t)\rangle = e^{-i\epsilon_{2k+1}t/\hbar}\sum_{n=-\infty}^{\infty}\sum_{\alpha}[e^{i(2n+1)\omega t}d_{1,2n+1}^{\alpha}(\epsilon_{2k+1})|\phi_g(r,R)\rangle|\chi_1^{\alpha}(R)\rangle + e^{i2n\omega t}d_{2,2n}^{\alpha}(\epsilon_{2k+1})|\phi_u(r,R)\rangle|\chi_2^{\alpha}(R)\rangle], \tag{5}$$

$$|\psi_{2k}^{+}(r,R,t)\rangle = e^{-i\epsilon_{2k}t/\hbar}\sum_{n=-\infty}^{\infty}\sum_{\alpha}[e^{i2n\omega t}d_{1,2n}^{\alpha}(\epsilon_{2k})|\phi_g(r,R)\rangle|\chi_1^{\alpha}(R)\rangle + e^{i(2n+1)\omega t}d_{2,2n+1}^{\alpha}(\epsilon_{2k})|\phi_u(r,R)\rangle|\chi_2^{\alpha}(R)\rangle]. \tag{6}$$

We label Floquet states in Eq. (5) as *odd* (with index $2k+1$) and Eq. (6) as *even* (with index $2k$), in view of the symmetry of the $|^2\Sigma_g^+\rangle$ (even) and $|^2\Sigma_u^+\rangle$ (odd) states [11].

The quasienergies ϵ_k have the property that for any integer p, $\epsilon_{k+p} = \epsilon_k + p\hbar\omega$. Therefore, solutions can be chosen to lie between 0 and ω. We must now take into account which Floquet states are created after a pulse rise from $f(t=0) = 0$ to $f(t=t_0) = 1$. The even states [Eq. (6)] can be connected adiabatically to the field-free state $|\phi_g\rangle$, while the odd states [Eq. (5)] can be connected to the $|\phi_u\rangle$ state. Thus, the even and odd quasienergies can be written as

$$\epsilon_{2k} \equiv \epsilon_{1,\alpha,2n} = \epsilon_{1,\alpha,0} + 2n\hbar\omega, \tag{7}$$

$$\epsilon_{2k+1} \equiv \epsilon_{2,\alpha,2n+1} = \epsilon_{2,\alpha,0} + 2n\hbar\omega. \tag{8}$$

It can be shown that a slow (adiabatic) rise will produce one Floquet state [12]. A rapid rise, such as we use here (linear rise over five cycles of the laser period), will produce a superposition of Floquet states:

$$|\Psi(r,R,t_0)\rangle = \sum_{k=-\infty}^{\infty} C_{2k+1}(t_0)|\psi_{2k+1}^{-}(r,R,t_0)\rangle + C_{2k}(t_0)|\psi_{2k}^{+}(r,R,t_0)\rangle, \tag{9}$$

$$C_{2k+1(2k)}(t_0) = \langle\psi_{2k+1(2k)}^{-(+)}(r,R,t_0)|\Psi(r,R,t_0)\rangle_{r,R}. \tag{10}$$

Once the superposition in Eq. (9) is created, the coefficients $C_k(t_0)$ remain constant, as long as the pulse shape remains constant. The dipole moment induced between t_0 and t is then

$$\begin{aligned} \mu^{\text{ind}}(t-t_0) &= \langle\Psi(r,R,t-t_0)|z|\Psi(r,R,t-t_0)\rangle_{r,R} \\ &= \sum_{k',k} C_{2k'+1}^{*}(t_0)C_{2k+1}(t_0)\langle\psi_{2k'+1}^{-}(r,R,t-t_0)|z|\psi_{2k+1}^{-}(r,R,t-t_0)\rangle_{r,R} \qquad (11) \\ &\quad + \sum_{k',k} C_{2k'}^{*}(t_0)C_{2k}(t_0)\langle\psi_{2k'}^{+}(r,R,t-t_0)|z|\psi_{2k}^{+}(r,R,t-t_0)\rangle_{r,R} \\ &\quad + 2\text{Re}\left\{\sum_{k',k} C_{2k'+1}^{*}(t_0)C_{2k}(t_0)\langle\psi_{2k'+1}^{-}(r,R,t-t_0)|z|\psi_{2k}^{+}(r,R,t-t_0)\rangle_{r,R}\right\} \qquad (12) \\ &= \mu_{--}^{\text{ind}} + \mu_{++}^{\text{ind}} + \mu_{+-}^{\text{ind}}, \qquad (13) \end{aligned}$$

where

$$\mu_{--}^{\rm ind} = \sum_{k',k} C_{2k'+1}^{*}(t_0) C_{2k+1}(t_0) e^{i(\epsilon_{2k'+1}-\epsilon_{2k+1})(t-t_0)/\hbar} \sum_{n',n} e^{-i2(n'-n)\omega(t-t_0)} \times \sum_{\beta,\alpha} [e^{-i\omega(t-t_0)} d_{1,2n'+1}^{\beta\,*}(\epsilon_{2k'+1}) d_{2,2n}^{\alpha}(\epsilon_{2k+1}) \mu_{1,\beta,2,\alpha} + e^{i\omega(t-t_0)} d_{2,2n'}^{\beta\,*}(\epsilon_{2k'+1}) d_{1,2n+1}^{\alpha}(\epsilon_{2k+1}) \mu_{2,\beta,1,\alpha}], \quad (14)$$

$$\mu_{++}^{\rm ind} = \sum_{k',k} C_{2k'}^{*}(t_0) C_{2k}(t_0) e^{i(\epsilon_{2k'}-\epsilon_{2k})(t-t_0)/\hbar} \sum_{n',n} e^{-i2(n'-n)\omega(t-t_0)} \times \sum_{\beta,\alpha} [e^{i\omega(t-t_0)} d_{1,2n'}^{\beta\,*}(\epsilon_{2k'}) d_{2,2n+1}^{\alpha}(\epsilon_{2k}) \mu_{1,\beta,2,\alpha} + e^{-i\omega(t-t_0)} d_{2,2n'+1}^{\beta\,*}(\epsilon_{2k'}) d_{1,2n}^{\alpha}(\epsilon_{2k}) \mu_{2,\beta,1,\alpha}], \quad (15)$$

$$\mu_{+-}^{\rm ind} = \sum_{k',k} C_{2k'}^{*}(t_0) C_{2k+1}(t_0) e^{i(\epsilon_{2k'}-\epsilon_{2k+1})(t-t_0)/\hbar} \sum_{n',n} e^{-i2(n'-n)\omega(t-t_0)} \times \sum_{\beta,\alpha} [d_{1,2n'}^{\beta\,*}(\epsilon_{2k'}) d_{2,2n}^{\alpha}(\epsilon_{2k+1}) \mu_{1,\beta,2,\alpha} + d_{2,2n'+1}^{\beta\,*}(\epsilon_{2k'}) d_{1,2n+1}^{\alpha}(\epsilon_{2k+1}) \mu_{2,\beta,1,\alpha}] + \text{c.c.} \quad (16)$$

The Fourier transform of Eq. (13) ($\mu^{\rm ind}(\omega_{\rm HG})$) gives the relationship between the HG spectrum and the quasienergies ϵ_{2k+1}. The dipole component between odd states, and between even states, give peaks at

$$\begin{aligned} \omega_{\rm HG}^{--} &= (\epsilon_{2k'+1} - \epsilon_{2k+1})/\hbar + (2m \pm 1)\omega \\ &= \epsilon_{2,\beta,0} - \epsilon_{2,\alpha,0} + (2m \pm 1)\omega, \\ \omega_{\rm HG}^{++} &= (\epsilon_{2k'} - \epsilon_{2k})/\hbar - (2m \pm 1)\omega \\ &= \epsilon_{1,\beta,0} - \epsilon_{1,\alpha,0} + (2m \pm 1)\omega, \end{aligned} \quad (17)$$

where $m = 0, \pm 1, \ldots, \pm\infty$. One obtains, therefore, split *odd* harmonic peaks; this would be the only result if the pulse rise were adiabatic, creating only one Floquet state (even or odd). If several Floquet states are excited by the pulse rise then transitions between even and odd states will produce additional peaks around *even* harmonic orders

$$\begin{aligned} \omega_{\rm HG}^{+-} &= (\epsilon_{2k'} - \epsilon_{2k+1})/\hbar + 2m\omega \\ &= \epsilon_{1,\beta,0} - \epsilon_{2,\alpha,0} + 2m\omega. \end{aligned} \quad (18)$$

If two quasienergies are degenerate, Eq. (18) shows that harmonic generation will be produced at exactly even harmonic orders.

The dependence of the HG spectrum on initial conditions is contained in the coefficients $C_k(t_0)$ in Eq. (12): photon emission will only occur between Floquet states which are populated by the rise of the pulse. This opens up the possibility of controlling the HG spectrum via the shape of the pulse rise, as has been discussed recently in the context of the two-level model [2,3]. The effects of pulse shape on photodissociation of H_2^+ have recently been reported by Aubanel *et al.* [13].

The relationship between HG and electronic field-molecule energy levels has been derived previously for the two-electronic-level model [1–4]. The difference in the case of the two-electronic-state problem with moving nuclei, treated here, is that we have vibronic quasienergies, and thus a HG spectrum with richer structure. This structure, if observed experimentally, would give direct evidence of laser-induced bound states in diatomic molecules, which so far have only been seen in numerical simulations [10,13–19]. Indirect evidence has appeared in above-threshold ionization experiments [20–22] and also in anomalous kinetic energy distributions of fragments arising from ATD (above-threshold dissociation) [23].

The inclusion of rotation in Eq. (13) is not complicated, as it simply requires summation over appropriate angular momenta and the inclusion of Clebsch-Gordan coefficients in the expression for the transition moment [Eq. (2)] [24].

One can calculate the quasienergies that appear in Eqs. (3)–(18) using either time-independent [6,7] or time-dependent methods. This latter approach has only appeared recently in the literature [25,26]. The idea is based on the spectral method for finding eigenvalues of time-independent Hamiltonians [27]. Here we have a periodically driven Hamiltonian, so the eigenvalues we obtain will be quasienergies of the Floquet Hamiltonian. One proceeds by evaluating an autocorrelation function of the total solution of the Schrödinger equation, Eq. (1), $\langle\Psi(t)|\Psi(t_0)\rangle$, or

$$\begin{aligned} G(t) &= \langle\phi_g|\langle\chi_1(t_0)\{|\phi_g\rangle|\chi_1(t)\rangle + |\phi_u\rangle\chi_2(t)\rangle\} \\ &= \langle\chi_1(R,t_0)|\chi_1(R,t)\rangle_R, \end{aligned} \quad (19)$$

where we have used the initial condition $\chi_2(t_0) = 0$. Clearly for the two-electronic-state model, the autocorrelation function reduces to autocorrelation of nuclear states only. We will take as initial wave function the nuclear eigenstate $|\chi_1^{\gamma}\rangle$ of the $^2\Sigma_g^+$ electronic potential:

$$|\Psi_0(r,R,t_0)\rangle = |\chi_1^{\gamma}\rangle|\phi_g\rangle. \quad (20)$$

Using expression (9) one obtains for the autocorrelation function

$$G(t) = \langle \phi_g(r,R) | \langle \chi_1^\gamma(R) | \Psi_0(r,R,t-t_0) \rangle$$
$$= \sum_k \left\{ e^{-i\epsilon_{2k+1}(t-t_0)/\hbar} C_{2k+1}^\gamma(t_0) \sum_n e^{i(2n+1)\omega(t-t_0)} d_{1,2n+1}^\gamma(\epsilon_{2k+1}) \right.$$
$$\left. + e^{-i\epsilon_{2k}(t-t_0)/\hbar} C_{2k}^\gamma(t_0) \sum_n e^{i2n\omega(t-t_0)} d_{1,2n}^\gamma(\epsilon_{2k}) \right\}, \quad (21)$$

where $C_k^\gamma(t_0) = \langle \psi_k | \chi_1^\gamma \rangle | \phi_g \rangle$. Spectral analysis of the Fourier transform $G(\omega)$ of Eq. (21) will yield peaks at $\epsilon_{2k+1}/\hbar - (2n+1)\omega$ and $\epsilon_{2k}/\hbar - 2n\omega$ [or $\epsilon_{2,\alpha,0}/\hbar - (2n+1)\omega$ and $\epsilon_{1,\alpha,0}/\hbar - 2n\omega$]. Note that if the initial ($t = t_0$) wave function had been chosen to be a combination of both electronic states, then one would have obtained overlapping peaks for $|\epsilon_{2,\alpha,0} - \epsilon_{1,\alpha,0}| \sim \hbar\omega$ ($\epsilon_{2,\alpha,0}/\hbar + n\omega$, $\epsilon_{1,\alpha,0}/\hbar + n\omega$). In order to apply this analysis (which applies to a periodic field) to the autocorrelation function obtained from the time-dependent calculation, Eq. (19), the calculation must be done using a periodic field, i.e., $\mathcal{E}_0 \sin(\omega t)$, with $|\chi_1(t=0)\rangle = |\chi_1^\gamma\rangle$ (an eigenfunction of the $^2\Sigma_g^+$ potential).

The above discussion has ignored the fact that, because of the presence of the nuclear continuum, the quasienergies (ϵ_k) are complex. The imaginary part gives the linewidth of the spectral feature centered on the real part [8,9,14]. Thus the above autocorrelation function analysis can yield energies and lifetimes of Floquet states.

In this section we have presented a *Floquet* analysis of harmonic generation by H_2^+. A *dressed state* analysis will be given in the next section. In the latter case, the Fourier index n and basis functions $d_{1,n}|\phi_g\rangle, d_{2,n}|\phi_u\rangle$ of Floquet theory are associated with the photon number and with *diabatic* (field-free) states, respectively, and the quasienergies ϵ_k are associated with nuclear eigenvalues of *adiabatic* field-molecule states.

III. RESULTS: NONROTATING H_2^+, FIXED AND MOVING NUCLEI

The results of two types of calculations are presented in this section, both for a 1064-nm laser. First, we present results of *exact* electronic calculations for nonrotating H_2^+ at a fixed internuclear distance of $R_f = 3$ Å (right turning point of $v = 13$). The same method as previously published was used, namely a Bessel-Fourier expansion coupled with a split-operator fast Fourier transform (FFT) method [1,28], and with a five cycle linear turn-on of the laser to a constant field, yielding the fixed nuclei electronic function $|\psi(R_f,r,t)\rangle$. Harmonic generation spectra were calculated by Fourier transforming the time-dependent dipole moment, $\mu^{\rm el}(R_f,t) = \langle \psi(R_f,r,t)|z|\psi(R_f,r,t)\rangle$, sampled between 6 and 60 cycles (21–213 fs) to reduce the background of the spectra due to transient states induced by the turn on of the pulse. A Hanning window function [$\sin(t\pi/T)^2$, where T is the length of the sample] was used before Fourier transformation to reduce leakage due to spurious sidebands and to reduce the background.

Second, we present results of *two-electronic-state* ($^2\Sigma_g^+$ and $^2\Sigma_u^+$) calculations for nonrotating H_2^+ (see Sec. IV for treatment of rotation), starting from diabatic (field-free) vibrational levels $v = 13$ and $v = 5$, using the same split-operator-FFT method as in previous publications [13,15,16,28]. The pulse shape is the same as above (unless specified otherwise), and the dipole moment is now

$$\mu^{\rm ind}(t) = \langle \chi_g(R,t)\phi_g(r,R) + \chi_u(R,t)\phi_u(r,R)|z|\phi_g(r,R)\chi_g(R,t) + \phi_u(r,R)\chi_u(R,t)\rangle$$
$$= {\rm Re}\langle \chi_g(R,t)|R|\chi_u(R,t)\rangle, \quad (22)$$

where r is the electronic coordinate and Re denotes the real part. We note that all laser-induced or stimulated processes are included in the time-dependent functions, whereas the dipole operator z corresponds to coherent spontaneous radiation emitted by the molecular ion (see discussion below).

Numerical calculations have shown that molecular photodissociation can be suppressed in the presence of strong laser fields, leading to molecular stabilization by a laser-induced avoided crossing mechanism [13,15–17]. Photodissociation probability P_d as a function of peak intensity is shown in Fig. 1 (circles) for H_2^+ in initial (rotationless) diabatic vibrational levels $v = 5$ or $v = 13$, with a 30 cycle flat pulse of a 1064-nm laser including a five cycle linear rise. Photodissociation is seen to rise (linearly initially, in accordance with the Fermi golden rule) to a maximum of 100%, followed by one or more minima. For the case of $v = 13$ there is a broad minimum between about 0.7×10^{14} W/cm^2 and 1.3×10^{14} W/cm^2 at about 70% dissociation, while for $v = 5$ there is a minimum of 85% dissociation at 1.2×10^{14} W/cm^2. It has been shown that such *stabilization* is due to trapping in laser-induced bound states [6,7,13,15–17] for which a semiclassical theory, analogous to the theory of molecular predissociation [29], has been developed. In Fig. 2 we show the diabatic potentials (solid lines) corresponding to states $V_g + 2p\hbar\omega$, $2p = n+2, n, n-2$, and $V_u + (2p-1)\hbar\omega$, $2p = n, n-2, n-4, n-6$ (n is the photon number), and the adiabatic potentials (dashed and dotted lines) obtained by diagonalizing the dressed state matrix containing the above diabatic potentials coupled by

$$\langle ^2\Sigma_u^+, n = 2m \pm 1 | \vec{d} \cdot \vec{E}_0/2 | ^2\Sigma_g^+, n = 2m \rangle = \hbar\Omega_R/2. \quad (23)$$

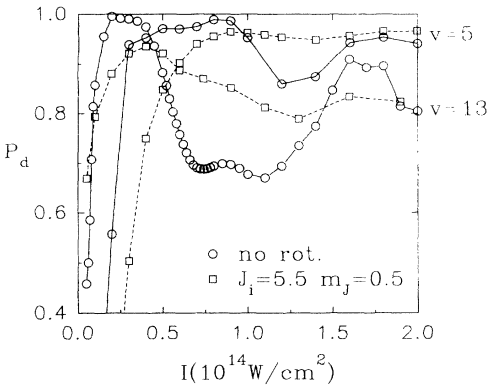

FIG. 1. Photodissociation probability for initial levels $v = 5, 13$ of H_2^+, with 30 cycle pulses (with five cycle linear rise) of 1064-nm radiation. Dashed line with squares (□): starting from $J_i = 5.5$, and for $m_J = 0.5$; solid lines with circles (o): no rotations.

The Rabi frequency Ω_R is defined in Eq. (2), and adiabatic potentials at 7.4×10^{13} W/cm^2 and 1.2×10^{14} W/cm^2, where P_d (Fig. 1) has minima, are shown in Fig. 2. The adiabatic potentials all have minima which can support at least one vibrational state, thus leading to stable states in intense fields. We note that Fig. 2 corresponds to Floquet states of one parity only (see Sec. II). The potentials $V_g + (n-1)\hbar\omega, V_u + (n-2)\hbar\omega$ corresponding to the Floquet states of the other parity, are redundant (even and odd Floquet states do not interact, see Sec. II) and are, therefore, not shown.

Next in Fig. 3(a) we show the harmonic generation spectrum at $I = 2.59 \times 10^{13}$ W/cm^2 from our exact, purely electronic, calculation with the nuclei fixed at $R_f = 3$ Å. This intensity corresponds to maximum dissociation (see Fig. 1). This spectrum is well reproduced up to the 9th harmonic by a two-level electronic-state calculation (with fixed nuclei) as shown in Fig. 3(b). This is because, in this case, the transition between the $^2\Sigma_g^+$ and $^2\Sigma_u^+$ states (the charge resonance transition) dominates the whole process. In fact, after a 60 cycle (213 fs) interaction with the laser pulse, only 1% of H_2^+ is ionized ($\langle\psi(t_f)|\psi(t_f)\rangle = \exp(-\Gamma t_f) = 0.99$ for $z < 128$ a.u., the component of the electronic coordinate along the internuclear axis). The corresponding ionization rate is $\Gamma = 2.3 \times 10^9\,\mathrm{s}^{-1}$. It is found that another 1% is excited to the upper excited states and 98% still remains in the lowest charge resonant states ($|c_1|^2 + |c_2|^2 = |\langle\psi(t_f)|^2\Sigma_g^+\rangle|^2 + |\langle\psi(t_f)|^2\Sigma_u^+\rangle|^2$). The spectrum of Fig. 3(b) is now well understood in a two-level, strong coupling (Rabi frequency $\Omega_R = 0.081 \gg \omega_0 = 0.019$, the energy separation) analysis [1–3]. In particular, the splitting Ω' at the frequencies $2n\omega \pm \Omega'$ in Fig. 3(a) and 3(b) has been shown to be given by the energy difference between Floquet states of the two-level model [Fig. 3(b)],

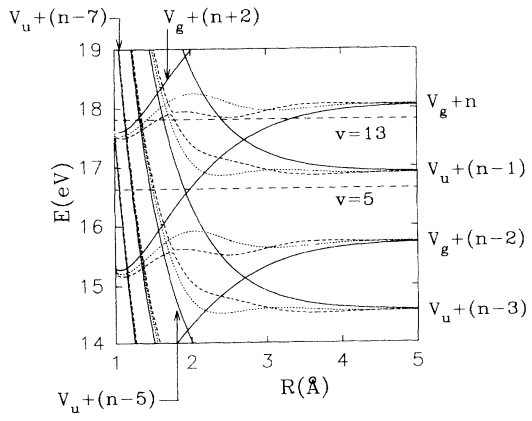

FIG. 2. Diabatic (field-free) (solid lines) and adiabatic field-molecule potentials for H_2^+ with $\lambda = 1064$ nm at intensities 7.4×10^{13} W/cm^2 (dotted lines) and 1.2×10^{14} W/cm^2 (dashed lines). Also shown are diabatic vibrational levels $v = 5, 13$. This figure corresponds to the even (odd) Floquet states for n even (odd). The numbers after the plus signs, e.g., $(n-7)$, are meant to be multiplied by $\hbar\omega$.

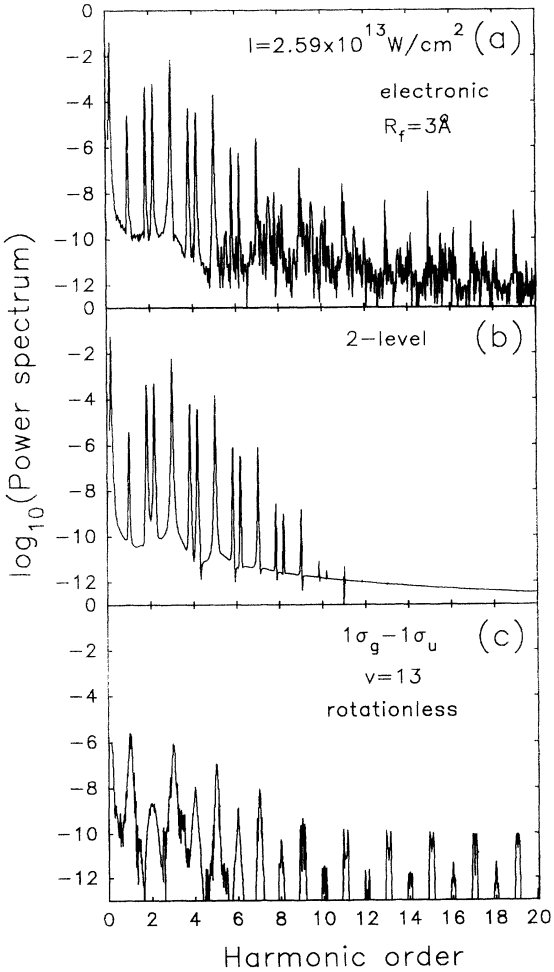

FIG. 3. Harmonic generation spectra of H_2^+ at $I = 2.59 \times 10^{13}$ W/cm^2, $\lambda = 1064$ nm, and 60 cycle pulse including five cycle linear rise. (a) exact electronic calculation (fixed nuclei) at $R_f = 3$ Å; (b) two-level model calculation at $R_f = 3$ Å; (c) two-electronic-state rotationless calculation with moving nuclei, starting from $v = 13$. This intensity corresponds to *maximum* dissociation (see Fig. 1).

given by a Bessel function: $\Omega' = \omega_0 J_0(2\Omega_R/\omega)$ [2]. Peaks beyond the 9th order in Fig. 3(a) are attributed to the upper level and continuum excitations. Figure 3(c) is the spectrum from a two-electronic-state ($1\sigma_g$ and $1\sigma_u$) moving nuclei calculation. The spectrum is seen to have lower efficiency and shows richer structure. These are explained next.

From Fig. 1 one can see why the HG spectrum in Fig. 3(c), which includes nuclear motion, is weaker than those in Figs. 3(a) and 3(b), which are purely electronic. Since dissociation is at its maximum and occurs rapidly at this intensity (reaching 99% by 70 fs), and since, furthermore, HG only occurs between nondegenerate electronic levels [1] (the $^2\Sigma_g^+$ and $^2\Sigma_u^+$ levels become degenerate for $R > 5$ Å, for which HG efficiency is zero), HG only occurs for a short time, resulting in weak and broad peaks in the spectrum. One predicts, therefore, that HG should be more efficient from $v = 13$ at a higher intensity where a minimum in P_d occurs, i.e., the stabilization regime. Figure 4 shows analogous results to Fig. 3, but for $I = 7.4 \times 10^{13}$ W/cm^2, where the minimum in P_d occurs. In this case, it is seen that the two-level fixed nuclei calculation [Fig. 4(b)] agrees reasonably well with the all-electronic fixed-nuclei calculation [Fig. 4(a)] up to the 11th harmonic. Higher-order peaks are more prominent in the latter due to upper level excitations and greater ionization: 26% of $H_2{}^+$ is ionized after a 60 cycle interaction with the laser pulse (ionization rate of $1.5\times10^{12}\,s^{-1}$). However the remaining (74%) nonionized part is mostly found in the $^2\Sigma_g^+$ (95%) and $^2\Sigma_u^+$ (4%) levels. The two-level moving-nuclei calculation is presented by Fig. 4(c). It is clear when compared to Fig. 3(c) that stabilization has increased HG efficiency about four orders of magnitude. Furthermore, there are more peaks in the results for moving nuclei [Fig. 4(c)] than in those for fixed nuclei Fig. 4(a) and 4(b), as would be expected since in the former case HG results from vibronic transitions, whereas in the latter case HG results from purely electronic transitions. Finally, we note that peaks around even harmonics are more closely spaced at this higher intensity.

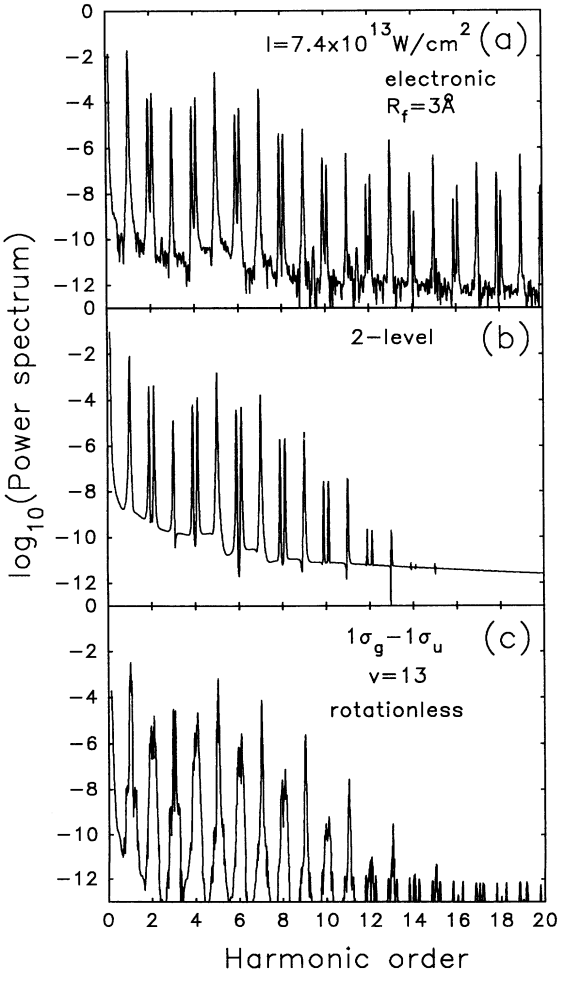

FIG. 4. Same as Fig. 3, except for $I = 7.4 \times 10^{13}$ W/cm^2. This intensity corresponds to *stabilization* of $v = 13$ (see Fig. 1), or minimum dissociation.

As discussed in Sec. II, the peaks in Figs. 3 and 4 can be assigned to differences between eigenvalues (quasienergies) ϵ_k of the Floquet Hamiltonian H_F [see Eqs. (17)–(18)]. We now analyze the HG spectra using the *dressed state* photon-molecule picture of quantum field theory. The two Hamiltonians (dressed and Floquet) can be shown to be equivalent in the limit of large photon number [30]. In the Floquet analysis of Sec. II, harmonic generation is obtained from the induced dipole moment given by a matrix element between levels of Floquet states of the same (odd harmonics) and of different (even harmonics) parity [Eq. (12)]. In the dressed analysis harmonic generation is obtained from an induced dipole moment given by a matrix element of an operator for coherent spontaneous emission between adiabatic states correlating asymptotically (large R) to dressed states differing in photon number n equal to the order of the harmonic [see Fig. 5 and Eq. (24) below]. In Fig. 5(a) we show the dressed adiabatic potentials from even and odd Floquet states at $I = 7.4 \times 10^{13}$ W/cm^2, whereas in Fig. 2 only Floquet states of one parity are shown. Also shown in Fig. 5(a) are bound states calculated using the autocorrelation method discussed in Sec. II. In Fig. 5(b) we show an enlargement of of the spectrum in Fig. 4(c), i.e., from a two-electronic-state moving-nuclei calculation at 7.4×10^{13} W/cm^2, $v = 13$, but now for a longer (200 cycle) pulse to allow better resolution of the peaks. We assign all peaks in the spectrum to transitions between these dressed levels of different parity [indicated by solid (even) and dashed (odd) lines in Fig. 5, for n even].

In particular, one observes from Fig. 5(a) that the transitions in the first harmonic region (a,b,c) occur between bound states in the shallow well created by the one-photon avoided crossings around $R = 3$ Å between potentials $V_g + n\hbar\omega$ and $V_u + (n-1)\hbar\omega$ [middle solid line in Fig. 5(a)], and between $V_g + (n-1)\hbar\omega$ and $V_u + (n-2)\hbar\omega$ [upper dashed line in Fig. 5(a)]. The first adiabatic potential correlates to $V_g + n\hbar\omega$, whereas the second correlates to $V_g + (n-1)\hbar\omega$. Thus, transitions a,b,c are determined by the coherent spontaneous electronic matrix element

$$\langle \phi_u, n-1, 0_k | z\hat{\mathcal{E}}_k | \phi_g, n-1, 1_k \rangle = \mu_{gu}(R) \langle 0_k | \hat{\mathcal{E}}_k | 1_k \rangle, \quad (24)$$

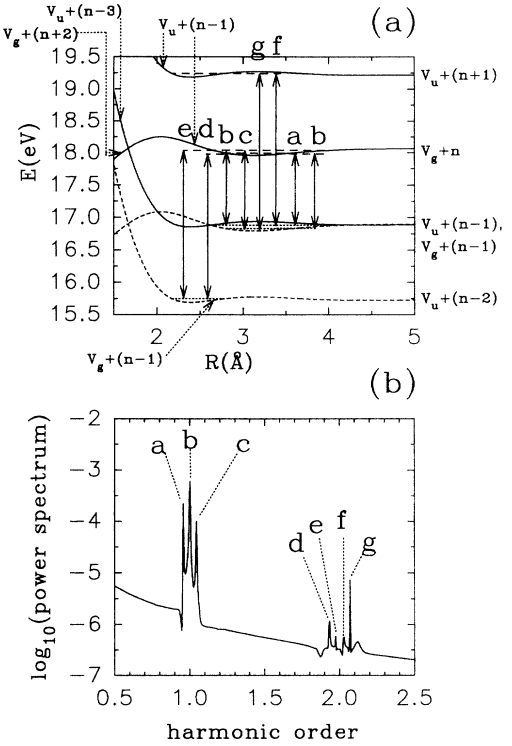

FIG. 5. (a) adiabatic field-electronic potentials corresponding to even (solid lines) and odd (dashed lines) Floquet states, for n even. One-photon avoided crossings occur at $R = 3.5$ Å, three-photon avoided crossings at $R = 2.5$ Å. Transitions between corresponding bound states of adiabatic wells correlate with peaks in spectrum of (b); (b) enlargement of HG spectrum in Fig. 4(c) ($I = 7.4 \times 10^{13}$ W/cm^2), except for 200 cycle pulse including five cycle linear rise.

i.e., between the electronic g and u diabatic components of the adiabatic electronic states around $R = 3$ Å. $\hat{\mathcal{E}}_k$ is the electric field operator giving rise to emission from the field vaccum $|0_k\rangle$ to the final one-photon state $|1_k\rangle$ of wave vector k. We note that the laser photon number, $n-1$, in the transition does not change, i.e., these photons give rise to dressing and hence creation of adiabatic states by continuous stimulated emissions and absorptions. It is the emitted photon number which changes by unity.

We clarify now the difference between Floquet harmonics as predicted by Eq. (12) and the dressed state harmonics as illustrated in Fig. 5. Equation (12) is obtained by evaluating the field-induced dipole moment $\mu^{\text{ind}}(t)$, Eq. (11), as the average value of z over Floquet states. Even harmonics are produced from transitions between Floquet states of different parity. The equivalent dressed state picture, involves spontaneous emission through the quantum matrix element [Eq. (24)] between diabatic states of the same laser photon number n [Fig. 5, or $n-1$, Eq. (24)]. These diabatic states are components of adiabatic states which correlate asymptotically to dressed states differing in photon number n corresponding to the order of the harmonic. As a result the dressed state representation shows the *direct* even harmonic photon transitions, i.e., $\epsilon_{k'} - \epsilon_k = n\hbar\omega$.

We note further that the spontaneous electronic transition moment alone, Eq. (24), is next to be multiplied by the Franck-Condon factor $\langle \epsilon_n^\alpha | \epsilon_{n-1}^\beta \rangle$ of the laser-induced adiabatic levels. Clearly, the overlap between these levels is excellent, as seen from Fig. 5(a), since the levels are trapped in similar wells, giving thus intense transitions in the first harmonic region. The d,e lines observed around the $2\hbar\omega$ [even harmonic region, Fig. 5(b)] are illustrated also in Fig. 5(a). These are caused by transitions between nuclear states with turning points on the repulsive $V_u + (n-1)\hbar\omega$ part of the adiabatic potential correlating to $V_g + n\hbar\omega$ (middle solid line potential) and nuclear states on the inner shallow well around 2.3 Å correlating to $V_u + (n-2)\hbar\omega$ (lowest dashed line potential). We note that these lower bound nuclear states are trapped in the upper adiabatic well formed by a three-photon avoided crossing between $V_u + (n-4)\hbar\omega$ and $V_g + (n-1)\hbar\omega$ potentials around $R = 2.3$ Å. The transition moment leading to emission in the even harmonic region in Fig. 5 would be Eq. (24) again. We note however that now the Franck-Condon factor is $\langle \epsilon_{n+1}^\alpha | \epsilon_{n-1}^\beta \rangle$, where ϵ_{n+1}^α is the adiabatic nuclear level in the well in the $R_e \simeq 3.5$ Å adiabatic potential correlating to $V_g + n\hbar\omega$. ϵ_{n-1}^β is the adiabatic nuclear level in the $R_e = 2.3$ Å adiabatic well correlating to $V_u + (n-2)\hbar\omega$. Clearly the overlap between these nuclear states is very poor as their wells have considerably different equilibrium positions ($R_e \simeq 3.5$ vs $R_e = 2.3$ Å). This explains the much weaker intensities of lines e,f,g,h in the $2\hbar\omega$ region in Fig. 5. Transitions f,g behave in a similar fashion, i.e., they are now due to transitions between the $V_u + (n-1)\hbar\omega$ part of the highest adiabatic potential in Fig. 5 [correlating to $V_u + (n+1)\hbar\omega$] with a minimum due to a three-photon avoided crossing between $V_u + (n-1)\hbar\omega$ and $V_g + (n-2)\hbar\omega$, and the adiabatic well correlating to $V_g + (n-1)\hbar\omega$. In conclusion, Fig. 5 illustrates that the structure in the *first* harmonic region is due to transitions between quasistable (due to nonadiabatic coupling with nuclear continuum states [9]) nuclear adiabatic levels trapped in the adiabatic wells created by one-photon avoided crossings around $R \simeq 3.5$ Å. The structure evident in the *second* harmonic region is due to transitions between adiabatic levels from the one-photon avoided crossings at $R \simeq 3.5$ Å and adiabatic levels trapped in adiabatic wells arising from three-photon avoided crossings at the shorter internuclear distance $R = 2.3$ Å. The overlap between these last states is small and hence unfavorable for second harmonic emission. This explains the weakness of the peaks in this region. Nevertheless, it is clear that the multiple photon avoided crossings illustrated in Figs. 2 and 5 can create stable adiabatic nuclear states which will enhance even harmonic generation [compare Figs. 3(c) and 4(c)].

Figure 6 shows the spectra from the same set of calculations as Fig. 4 ($v = 13$ or $R_f = 3$ Å) but at intensity $I = 1.2 \times 10^{14}$ W/cm^2, i.e., on the rising dissociation curve for $v = 13$, but at a minimum of P_d for $v = 5$ (Fig. 1). It is seen that the spectrum of Fig. 6(b) (the two-electronic-level fixed-nuclei calculation) differs from that of Fig. 6(a) (the all-electronic fixed-nuclei cal-

culation) quantitatively, even for low-order harmonics. The strengths of high-order harmonics in Fig. 6(a) approach those of the lower-order harmonics, when compared with the lower intensity cases (Figs. 3 and 4). At intensity $I = 1.2 \times 10^{14}$ W/cm^2, a large amount of ionization occurs after a 60 cycle interaction with the laser pulse (97% of H_2^+ is ionized, corresponding to a rate of 1.7×10^{13} s^{-1}). It is recently understood that the ionized electrons contribute to high-order harmonic generation via reinteraction with the parent ion en route to ionization [3]. We therefore conclude that for intensities beyond 10^{14} W/cm^2, the two-level model is no longer valid. The spectrum from the two-electronic-level moving-nuclei calculation is shown in Fig. 6(c). As in Fig. 5, the peaks in the HG spectrum of Fig. 6(c) can be assigned to transitions between dressed energy levels. Notice that here pure even harmonics are produced, as there are dressed states which are separated by exactly twice the photon energy.

Consider now what happens when H_2^+ is initially in the $v = 5$ vibrational state. This vibrational level is at the three-photon crossing point (Fig. 2), and thus dissociates rapidly with very little trapping. This contrasts with the cases above with $v = 13$, which is above the one-photon crossing, and thus can become trapped in the adiabatic potential which converges to $V_g + n\hbar\omega$, and can also transit nonadiabatically to other adiabatic wells. Photodissociation from $v = 5$ can be trapped to a small extent, for $I > 10^{14}$ W/cm^2, in an adiabatic well (correlating to $V_g + n\hbar\omega$) created at small R by the three- and five-photon crossings ($R \leq 2$ Å, Fig. 2). This results in a minimum in P_d at $I = 1.2 \times 10^{14}$ W/cm^2 in Fig. 1, and $P_d < 1.0$ at higher intensities. The HG spectrum at the same conditions as Fig. 6(c), but now for $v = 5$, is shown in Fig. 7, i.e., at $I = 1.2 \times 10^{14}$ W/cm^2, which corresponds to the minimum in P_d. There are two differences between the two figures. First, the intensities of the odd harmonics are lowered by on average one order of magnitude in Fig. 7, but the relative intensities of the odd harmonics is about the same. This happens because the $v = 5$ case has a higher-order coupling (third order) between the electronic states than the $v = 13$ case (one-photon coupling), but nevertheless a higher photodissociation rate (see Fig. 1). Second, the even harmonics have almost completely disappeared in Fig. 7. This can be understood from Eq. (12), or more particularly the overlap integral, Eq. (10). Since the pulse rise is short (five cycles) we can assume that $\Psi(t_0)$ ($t_0 = 5$ cycles) is very similar to the initial $v = 5$ wave function at $t = 0$. One can see from Fig. 2 that one of the pair of adiabatic potentials at 1.2×10^{14} W/cm^2 [dashed lines; e.g., extending assymptotically to $V_u + (n-1)\hbar\omega$] has a shallow well between 3 and 4 Å, which does not overlap with the initial $v = 5$ wave function [and therefore with $\Psi(t_0)$] which has its right turning point at about 2 Å. Therefore, from Eq. (12) and Fig. 2, only transitions between vibrational levels of the other adiabatic potential (with a minimum between 1 and 3 Å) are permitted, yielding only odd harmonics, as seen in Fig. 7. The effect of rapid dissociation or conversely trapping on harmonic generation is the same here as for the case with $v = 13$. A harmonic generation spectrum, not shown here, at $I = 9 \times 10^{13}$ W/cm^2 corresponding to a maximum in P_d (=0.99), yields a very weak spectrum, as was the case in Fig. 3(c) for maximum dissociation, P_d, for $v = 13$.

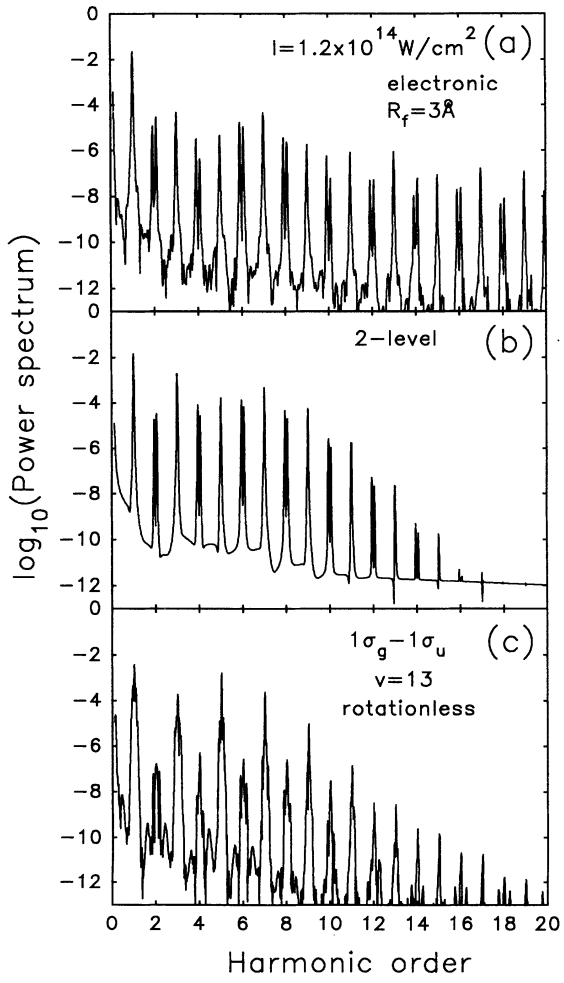

FIG. 6. Same as Fig. 3, except for $I = 1.2 \times 10^{14}$ W/cm^2, corresponding to another intensity where $v = 13$ is stabilized (see Fig. 1).

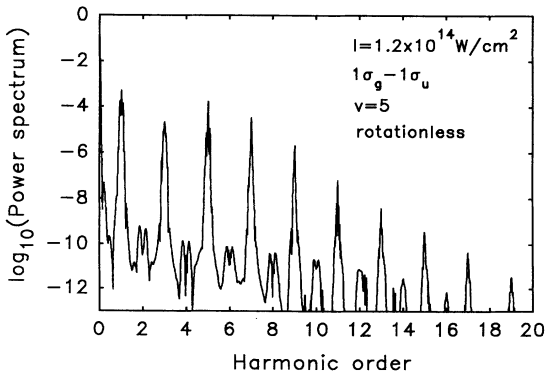

FIG. 7. Same as Fig. 6(c), except for initial vibrational state $v = 5$. This intensity corresponds to stabilization of $v = 5$ (see Fig. 1).

IV. RESULTS: ROTATING H_2^+

We wish next to examine the effect of rotational excitation on harmonic generation. The effect of rotational excitation on stabilization and angular distribution in the photodissociation of H_2^+ has been addressed by us recently [15,16], for other wavelengths (213 and 769 nm). Here we use the same approach in treating rotations: we take as initial state the rotational level $J = N + 0.5 = 5.5, m_J = 0.5$ (this state is parallel to the field and undergoes maximum radiative coupling) and expand the total two-electronic-state wave function [Eq. (22)] into rotational states:

$$\Psi(r,R,\theta,t) = \sum_{N=0}^{N_{\max}} \chi_{J,m_J}(R,t)\phi_J(r,R) \times \left(\frac{2J+1}{4\pi}\right)^{1/2} D^{J^*}_{m_J,1/2}(\phi,\theta,0) \qquad (25)$$

where $D^{J^*}_{m_J,1/2}(\phi,\theta,0)$ is the rotation matrix [24], $\phi_J(r,R) = |^2\Sigma_g^+\rangle$ for odd rotational quantum number N, $\phi_J(r,R) = |^2\Sigma_u^+\rangle$ for even N, and $\chi_{J,m_J}(R,t)$ is the nuclear function which propagates on the potential $V_g(R)+V_r(R,N)$ for odd N and on $V_u(R)+V_r(R,N)$ for even N; $V_r(R,N)$ is the rotational centrifugal potential:

$$V_r(R,N) = \hbar^2 N(N+1)/(2\mu R^2). \qquad (26)$$

Up to 40 rotational states were required in the expansion to obtain converged results for intensities $10^{13} \le I \le 10^{14}$ W/cm^2.

Consider first the effect of rotational excitation on stabilization of photodissociation by a 1064-nm laser (Fig. 1). One can see that rotation either stabilizes or destabilizes photodissociation, as has been seen and explained before [10,15,16]. The $^2\Sigma_g^+$ and $^2\Sigma_u^+$ potentials are modified by the centrifugal energy, Eq. (26). This modification creates multiple N-dependent laser-induced avoided crossings, which can lead to increased stabilization compared with the rotationless case [10], but it can also destabilize the rotationless laser-induced bound states, by destroying potential wells.

In Fig. 1, one notices the same relative effect of rotations on three-photon and one-photon resonant photodissociation as was seen recently by us in calculations on H_2^+ with $\lambda = 769$ nm [16]: three-photon resonant dissociation is completely destabilized, whereas one-photon resonant stabilization is enhanced or reduced by rotational excitation. The three-photon case was explained previously by us as resulting from initial quick rotational pumping as the system achieves resonance, thus creating a superposition of many rotational states each with a different lifetime. What is different in the present $\lambda = 1064$ nm excitation, is that the laser-induced potential well in the vicinity of the $V_g + n\hbar\omega - V_u + (n-1)\hbar\omega$ one-photon crossing ($R = 3$ Å) persists beyond 10^{14} W/cm^2 (dashed line, Fig. 2), unlike the case with $\lambda = 769$ nm, where the analogous well disapears by 5×10^{13} W/cm^2; this explains why the one-photon stabilization persists past 10^{14} W/cm^2 for $\lambda = 1064$ nm ($v_i = 13$, Fig. 1), and not for $\lambda = 769$ nm [16].

Before examining the effect of rotations on HG, we will examine the distribution over rotational states at the end of the 60 cycle laser pulse, for $v = 13$ and $I = 2.59 \times 10^{13}$ W/cm^2 [Fig. 8(a), no trapping in rotationless results] and 7.4×10^{13} W/cm^2 [Fig. 8(b), some trapping in rotationless results]. Also shown in bold in Fig. 8 is the rotational state distribution of the undissociated part of the wave function, i.e., the total wave function [Eq. (25)] integrated between $R = 0$ and 5 Å. The final rotational populations are distributed over odd and even values of N (recall that initially, $N = 5$), reflecting the fact that dissociation occurs into the $V_u + (n-1)\hbar\omega$ and $V_g + (n-2)\hbar\omega$ channels. The first corresponds to direct one-photon dissociation induced by the nondiabatic coupling at the one-photon avoided crossing at $R = 3$ Å. The second corresponds to ATD, i.e., $v = 13$ transits to $V_u + (n-3)\hbar\omega$ after a three-photon absorption; the nuclear wave packet thus created encounters the one-photon avoided crossing between $V_g + (n-2)\hbar\omega$ and $V_u + (n-3)\hbar\omega$, thus leading to final photodissociation fragments in high energy continuum states of the ground state, i.e., the $V_g + (n-2)\hbar\omega$ potential. This phenomenon was confirmed experimentally by Bucksbaum *et al.* [31] and then numerically by Bandrauk *et al.* [18] and He *et al.* [19]. Notice that in Fig. 8(b), for the higher intensity stabilization region, the distribution is more concentrated at smaller values of N. In fact, Fig. 8(a) seems to exhibit a bimodal distribution with

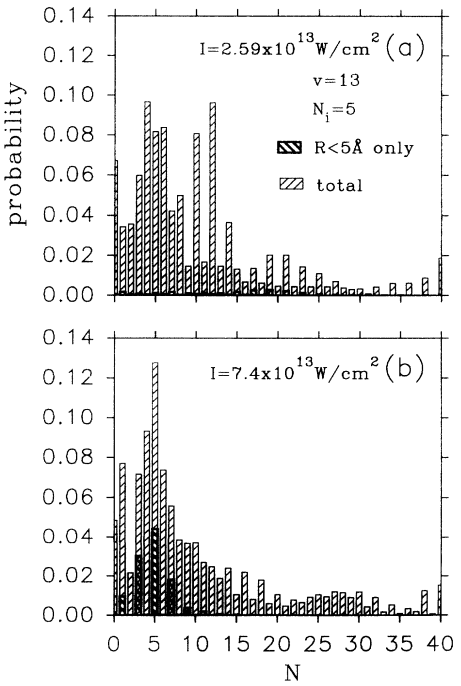

FIG. 8. Final distribution over rotational states, from two-electronic-state calculation, starting from $v = 13$, $N_i = 5$, and for intensities (a) 2.59×10^{13} W/cm^2 (maximum dissociation) and (b) 7.4×10^{13} W/cm^2 (minimum dissociation). Also shown in bold is final distribution for total wave function integrated between 0 and 5 Å.

maxima at $N \simeq 4$ and 12 for $I = 2.59 \times 10^{13}$ W/cm^2. The reason can be found in the accommodation of rotational states in adiabatic wells. At the lower intensity (2.59×10^{13} W/cm^2) there are no stable adiabatic wells present, so dissociation into the one- and two-photon channels occurs, after multiple stimulated absorption and emission steps which leads to climbing of the rotational ladder. At the higher intensity (7.4×10^{13} W/cm^2) stable adiabatic wells exist (Figs. 2 and 5), which support only a small number of rotational states. Using the centrifugal potential, Eq. (26), evaluated at the equilibrium position of the adiabatic well (R_{ae}) one can estimate the number of rotational states N_s which can be accommodated by the ground vibrational state (E_{ga}) of the adiabatic well [depth $E_D = E(R = \infty) - E_{ga}$], i.e., solving $E_D = V_r(R_{ae}, N_s)$ for N_s: $N_s = 13$ for the well correlating to $V_g + n\hbar\omega$ ($R_{ae} = 3.2$ Å, $E_{ga} = 17.99$ eV, $E_D = 0.07$ eV), and $N_s = 7$ for the well correlating to $V_u + (n-1)\hbar\omega$ ($R_{ae} = 2.3$ Å, $E_{ga} = 16.91$ eV, $E_D = 0.03$ eV). Dissociation can still occur into high rotational states, as in Fig. 8(a), but the states which remain trapped must have low N; this is shown in Fig. 8(b) (bold), where the undissociated ($R < 5$ Å) part of the wave function is confined to $N < 10$. Similar occupation of low N values was seen in all other cases at high ($> 5 \times 10^{13}$ W/cm^2) intensity. The net result is trapping in rotational states N lower than about 10 at high intensity. Thus one can see that nuclear trapping not only reduces photodissociation, but can also reduce rotational excitation when the field-free potential wells only support a small number of rotational states.

Consider now the HG spectrum for H_2^+ with rotation in $v = 13$, $J = 5.5, m_J = 0.5$ at 2.59×10^{13} W/cm^2, Fig. 9(a), where maximum dissociation occurs for the rotationless case (Fig. 1). The first and second harmonic peaks are enhanced while the higher-order peaks are the same or reduced in intensity, compared to the rotationless spectrum [Fig. 3(c)]. Higher intensity is expected for the rotational results at this lower field intensity, because of the lower dissociation rate when rotation is present (Fig. 1). However, rotational excitation can also compete with HG, decreasing the intensity of the HG spectrum. To expand on this latter point, the maximum energy acquired by an electron on moving from proton A to B in H_2^+ has been recently shown to be twice the Rabi frequency [Eq. (2)] $2\hbar\Omega_R = eRE$, where E is the field strength [1], i.e., this is the potential energy difference between the two nuclei in a laser field E. Taking rotation into account, in the limit of large J, this maximum energy becomes reduced to $2\hbar\Omega_R[(J+1+m_J)(J+1-m_J)]^{1/2}/2(J+1) \sim \hbar\Omega_R$. For H_2^+ fixed at the turning point of $v = 13$ ($R = 3.2$ Å), and using the rigid rotor expression for the rotational energy [Eq. (26) at $R = R_e = 1.06$ Å], we plot the maximal value of the rotational quantum number ($N_{\max}$) pumped by the expected maximum Rabi energy $\hbar\Omega_R$, as a function of intensity in Fig. 10, along with the number of rotational states ($N_{\rm rot}$) populated (to 90% of the total probability) by the end of the pulse in the calculations corresponding to the dashed curve for $v = 13$ in Fig. 1. At 2.59×10^{13} W/cm^2, where maximum dissociation occurs, $N_{\rm rot} = 20$ and $N_{\max} = 25$. Therefore, most of the available energy is taken up by rotational excitation. This result was predicted earlier by Bandrauk and Claveau using a diffusion model [32]. For higher intensity $N_{\rm rot}$ has a cutoff around $N \simeq 10$, because of the effect of stabilization by trapping in laser-induced wells. Therefore the excess energy can be taken up by the electrons to generate HG. Thus one expects that when stabilization reduces the extent of rotational excitation, the competition of the latter with HG will be minimized.

The HG spectrum for H_2^+ in $v = 13$, $J = 5.5, m_J = 0.5$ at 7.4×10^{13} W/cm^2, where now minimum dissociation occurs without rotation, is shown in Fig. 9(b) including rotation. The intensity of the odd harmonics is reduced by less than an order of magnitude, compared to the rotationless case [Fig. 4(c)], because of the increase in the photodissociation probability induced by rotations (see Fig. 1). The even harmonics, which we have shown above to occur when there exist adiabatic field-induced

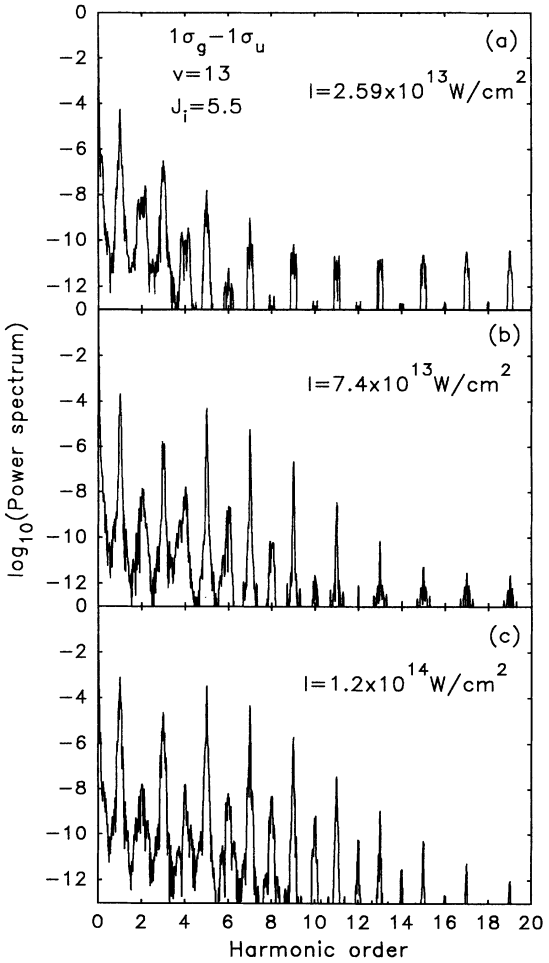

FIG. 9. HG spectrum for same conditions as (a) Fig. 3(c) (2.59×10^{13} W/cm^2, maximum dissociation), (b) Fig. 4(c) (7.4×10^{13} W/cm^2, minimum dissociation), (c) Fig. 6(c) (1.2×10^{14} W/cm^2, another dissociation minimum); except now with full rotational treatment, starting from $v = 13$, $J = 5.5$, and for $m_J = 0.5$.

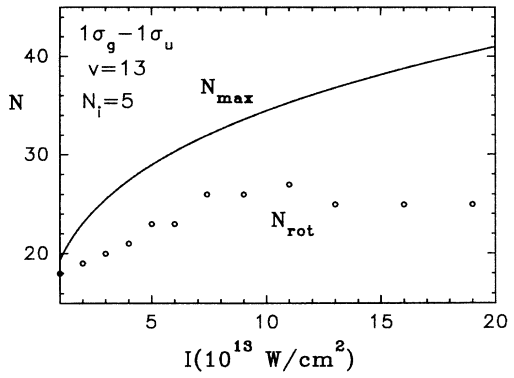

FIG. 10. Maximum rotational quantum number, $N_{\max}$, determined from Rabi energy $\hbar\Omega_R$ (solid line) at $R = 3.2$ Å, and number of rotational states excited to 90% of total probability, $N_{\rm rot}$ (symbols), obtained from rotational calculation at $v = 13$ and initial $N_i = 5$ (see Fig. 1 for parameters).

bound states separated by twice the photon energy, are reduced by more than an order of magnitude. Recall our discussion above of the number of rotational states accommodated by the adiabatic potentials: one of the pair [correlating to $V_u + (n-1)\hbar\omega$] can only contain rotational states up to $N = 7$, whereas the other (correlating to $V_g + n\hbar\omega$) can contain up to $N = 13$. Recall also that our initial condition is $N = 5$. Therefore, very little trapping will occur in the adiabatic well correlating to $V_u + (n-1)\hbar\omega$ compared to the amount trapped in the other well, and the condition of two populated wells differing by twice the photon energy will not be fulfilled. Similar results are seen in Fig. 9(c), at 1.2×10^{14} W/cm^2, when compared with the rotationless case, Fig. 6(c). The detailed structure around each harmonic order is similar to the rotationless case, but now broadened because of the presence of rotational branches in the spontaneous emission. We were not able to resolve these branches, because of the prohibitive computational resources required. In general with rotation, lower effiencies in photon emission are observed, due to the destabilizing effect introduced by the laser pumping of angular momentum.

V. CONCLUSION

We have shown in this paper that it is essential to include nuclear degrees of freedom in analysis of harmonic generation by the H_2^+ molecule. Such degrees of freedom give rise to structure in the harmonic generation (HG) spectra at even and odd harmonic orders, which can be assigned to photon emission between dressed states of the field-molecule system. Previous work on HG of H_2^+ with fixed nuclei showed that even-order HG is possible at strong fields which break the symmetry of the molecule by appropriate linear combination of the two charge resonance states, $^2\Sigma_g^+$ and $^2\Sigma_u^+$ [1–4]. This prediction is confirmed here when nuclear motion is taken into account, and enhanced by the presence of new laser-induced adiabatic bound states. The assignment of low-order harmonics (less than 10th order) to these two charge resonance states, in the case where the nuclei are stretched to 3 Å, is confirmed here for intensities less than 10^{14} W/cm^2. At intensities higher than 10^{14} W/cm^2, higher electronic excitation and ionization dominate.

In order for a purely electronic analysis to be valid, the nuclei must remain fixed during the duration of the pulse. This can be accomplished in the case of a light molecule such as H_2^+ by trapping the nuclei in field-induced potential wells. Such trapping can be achieved at intensities lower than 10^{14} W/cm^2 (at higher intensities a two-electronic-state description is no longer valid), by the one- and three-photon avoided crossings for $v = 13$ (Figs. 2 and 5). The HG spectra of stabilized H_2^+ have a close resemblance to the fixed nuclei spectra: the relative intensities of even and odd harmonics is the same. But it is what is different that is interesting: rich structure that is direct evidence for the presence of laser-induced bound states. Rotational motion can spoil spectra by destabilizing nuclear trapping, and thus increasing photodissociation at the expense of HG. In particular, we have seen here that rotational excitation reduces even harmonics, because of preferential population of one laser-induced potential and less of the other between which emission occurs. It is the presence of bound states of these wells separated by twice the photon frequency that gives rise to even harmonics. Rotational motion also broadens the structure of the HG peaks.

Fixed nuclei calculations, e.g., Figs. 6(a) and 6(b), show even harmonics which are split, $2\omega \pm \Omega$, where Ω is a high-order Rabi frequency shift. Introducing nuclear motion, one has now the possibility of creating adiabatic states as a result of laser-induced crossings. These new states now allow the possibility of photon emission at exactly the even harmonic frequency 2ω. Such even harmonics should be detectable since, in general, they will enhance their intensity by coherent cooperative effects. We must emphasize that all our calculations are single-molecule calculations, therefore, we have neglected phase matching which will enhance even and odd harmonics but not the Raman-like side bands [33]. Clearly, the presence of significant even harmonics in molecular HG would be a signature of molecular stabilization by laser-induced avoided crossings.

Diatomic molecular ions are a good potential source for high harmonic generation (up to 100th order) [1]. The high energy portion is attributable to reinteraction of the ionizing electron with the remaining core [3]. The low energy portion, which has higher efficiency, results from the strongly coupled change-resonance states ($1\sigma_g$-$1\sigma_u$), which for H_2^+ nuclei stretched to 3 Å, are well isolated. To observe the lower harmonics the nuclei must be frozen, either inertially, in the case of heavy nuclei, or by nuclear stabilization, as we have presented here. Harmonic generation from stabilized nuclei exhibit structure, which, if observed experimentally, would provide the first direct evidence of nuclear stabilization due to laser-induced bound states; in effect one would be doing intense-field molecular spectroscopy, where what is being observed is the bound states of potentials modified by the field, as first predicted by Bandrauk and Turcotte [10], and not

the field-free potentials. Finally, we have examined only one type of pulse, a linear rise to constant field. It should be possible to control the harmonic generation by stabilized molecular ions, by varying the shape of the pulse rise, as has been shown recently in the context of two-level systems [2,3].

ACKNOWLEDGMENTS

We thank the Natural Sciences and Engineering Research Council of Canada and the National Centre of Excellence in Molecular Dynamics for supporting this research.

[1] T. Zuo, S. Chelkowski, and A. D. Bandrauk, Phys. Rev. A **48**, 3837 (1993).
[2] M. Yu. Ivanov, P. B. Corkum, and P. Dietrich, Laser Phys. **3**, 375 (1993); M. Yu. Ivanov and P. B. Corkum, Phys. Rev. A **48**, 580 (1993).
[3] P. B. Corkum, Phys. Rev. Lett. **71**, 1994 (1993).
[4] L. Playa and L. Roso-Franco, J. Opt. Soc. Am. B **9**, 2210 (1992).
[5] R. S. Mulliken, J. Chem. Phys. **7**, 20 (1939).
[6] J. M. Yuan and T. F. George, J. Chem. Phys. **68**, 3040 (1978).
[7] A. D. Bandrauk and M. L. Sink, Chem. Phys. Lett. **57**, 569 (1978); J. Chem. Phys. **74**, 1110 (1981).
[8] A. D. Bandrauk and J. F. McCann, Comments At. Mol. Phys. **22**, 325 (1989).
[9] See, e.g., A. D. Bandrauk, *Molecules in Laser Fields* (Dekker, New York, 1993).
[10] A. D. Bandrauk and G. Turcotte, J. Chem. Phys. **77**, 3867 (1982); J. Phys. Chem. **87**, 5098 (1983).
[11] N. L. Manakov, V. D. Ovsiannikov, and L. P. Rapoport, Phys. Rep. **141**, 319 (1986).
[12] C. Cohen-Tannoudji, J. Dupont-Roc, and G. Grynberg, *Photons and Atoms* (Wiley, New York, 1989).
[13] E. E. Aubanel, A. D. Bandrauk, and P. Rancourt, Chem. Phys. Lett. **197**, 419 (1992).
[14] A. D. Bandrauk, E. E. Aubanel, and J. M. Gauthier, Laser Phys. **3**, 381 (1993).
[15] E. E. Aubanel, J. M. Gauthier, and A. D. Bandrauk, Phys. Rev. A **48**, 2145 (1993).
[16] E. E. Aubanel, A. Conjusteau, and A. D. Bandrauk, Phys. Rev. A **48**, 4011 (1993).
[17] A. Giusti-Suzor and F. H. Mies, Phys. Rev. Lett. **68**, 3869 (1992).
[18] A. D. Bandrauk, E. Constant, and J. M. Gauthier, J. Phys. (France) II **1**, 1033 (1991); A. D. Bandrauk and J. M. Gauthier, J. Opt. Soc. Am. B **7**, 1420 (1990).
[19] X. He, O. Atabek, A. Giusti-Suzor, and F. Mies, Phys. Rev. Lett. **64**, 515 (1990).
[20] J. W. J. Verschuur, L. D. Noordham, and H. B. van Linden van den Heuwell, Phys. Rev. A **40**, 4383 (1989).
[21] S. W. Allendorf and A. Szöke, Phys. Rev. A **44**, 518 (1991).
[22] A. Zavriyev, P. H. Bucksbaum, J. Squier, and F. Salin, Phys. Rev. Lett. **70**, 1077 (1993).
[23] A. Zavriyev and P. H. Bucksbaum, in *Molecules in Laser Fields*, edited by A. D. Bandrauk (Dekker, New York, 1993), Chap. 2.
[24] R. N. Zare, *Angular Momentum* (Wiley, New York, 1988).
[25] R. Bavli and H. Metiu, J. Chem. Phys. **98**, 6632 (1993).
[26] T. Millack, V. Véniard, and J. Henkel, Phys. Lett. A **176**, 433 (1993).
[27] M. D. Feit, J. A. Fleck, Jr., and A. Steiger, J. Comput. Phys. **47**, 412 (1982); M. R. Hermann and J. A. Fleck, Jr., Phys. Rev. A **38**, 6000 (1988); M. Horbatsch, J. Phys. B **24**, 4919 (1991).
[28] A. D. Bandrauk and H. Shen, J. Chem. Phys. **99**, 1185 (1993).
[29] A. D. Bandrauk and M. S. Child, Mol. Phys. **19**, 95 (1970).
[30] F. H. M. Faisal, *Theory of Multiphoton Processes* (Plenum, New York, 1988), Chap. 10.
[31] P. H. Bucksbaum, A. Zavriyev, H. G. Muller, and D. W. Schumacher, Phys. Rev. Lett. **64**, 1883 (1990).
[32] A. D. Bandrauk and L. Claveau, J. Phys. Chem. **93**, 107 (1989).
[33] Y. R. Shen, *The Principles of Nonlinear Optics* (Wiley, New York, 1984).